Received: 11 January 2016 | Revised: 16 December 2016 | Accepted: 5 February 2017

DOI 10.1002/etep.2352

RESEARCH ARTICLE

WILEY

# Virtual flux direct power-backstepping control of 5-level T-type multiterminal VSC-HVDC system

**Ahmed Reguig Berra**[1] | **Said Barkat**[1] | **Mansour Bouzidi**[2,3]

[1] Laboratoire de Génie Electrique, Facultéde Technologie, Université Mohamed Boudiaf, M'Sila 28000, Algeria

[2] Département de l'Electronique et des Communications, Faculté des Nouvelles Technologies d'Information et Communication, Université Kasdi Merbah, Ouargla 30000, Algeria

[3] Département d'Electrotechnique, Faculté des Sciences de l'Ingénieur, Université Djillali Liabes de Sidi Bel Abbes, Sidi Bel Abbes 22000, Algeria

**Correspondence**
Ahmed Reguig Berra, Laboratoire de Génie Electrique, Facultéde Technologie, Université Mohamed Boudiaf, M'sila 28000, Algeria.
Email: berra.ahmed@univ-msila.dz

**Summary**

In this study, a nonlinear control of a 5-level T-type converter topology-based multiterminal voltage source converter high-voltage direct current system is proposed. The idea of the proposed control is to combine the backstepping control and direct power control with virtual flux concept into one controller able to improve the performance of the transmission system. In the other side, the use of a 5-level space vector modulation with a balancing strategy based on effective use of the redundant switching states of the converters voltage vectors guarantees the objective of maintaining balanced voltages in DC-capacitors. Finally, simulations of the 5-level T-type multiterminal voltage source converter high-voltage direct current system validate the effectiveness of the proposed control law. The obtained results are compared with those performed by a conventional Proportional Integrator (PI) controller. These outcomes allow to exhibit excellent transient response during a range of operating conditions.

**KEYWORDS**

backstepping control, five-level T-type converter, multilevel space vector modulation, multiterminal high-voltage direct current, virtual flux direct power control

## 1 | INTRODUCTION

With the development of renewable energy sources, there is an urgent need to integrate decentralized and relatively small-scale power stations in the network with the objective to offer technical, economical, and environmental benefits.[1]

Among the renewable generation technologies, offshore wind farms (OWF) promise to become an important energy source in the near future.[2] The connection to the OWF can be either via a high-voltage alternating current transmission system or via a high-voltage direct current (HVDC) transmission system.

Nowadays, the dominant transmission technology is still the classical AC transmission.[3] However, it suffers from several disadvantages such as the existence of reactive power flow and the difficulty in controlling the power flow and guaranteeing the network's stability.[4,5] Compared with high-voltage alternating current transmission system, HVDC technology is gaining much attention in the power sector, and it is recognized as a suitable solution for OWFs located more than 50 km from shore. This is primary because once the cable is charged, almost its entire current carrying capacity is available for real power transfer and the possibility of interconnecting asynchronous networks. Furthermore, in this kind of transmission system, the power control through a DC link is fast and precise, and the DC links are reliable and can improve transient stability and dynamic damping of electrical system oscillations.[4,6–8]

On the other hand, line commutated converter and voltage source converters (VSCs) are the 2 main types of converter technology used in HVDC transmission systems.[6] However, the conventional HVDC using thyristor technology has several drawbacks limiting the range of its application.[7] The thyristor cannot be turned off with gate signal directly; the power flow reversal with line commutated converter HVDC is limited and is performed by changing the DC voltage polarity, and besides all these, the reactive power required to the thyristor valves in the converter.[7,9,10]

  

Recent developments in semiconductor technology of high-power switches, eg, insulated gate bipolar transistor, have resulted in a widespread acceptance of the VSC for high-power applications.[11] The benefits of using VSC are independent control of both active and reactive power, high-dynamic performance, and multiterminal possibility. In addition, VSC has other positive aspects such as power reversal without changing DC voltage polarity, possibility of static synchronous series compensation characteristics, no need of reactive power compensators, and no line commutation problems.[6,11,12]

Transmitting electrical energy across long distances between nodes of an interconnected network can be accomplished by a point-to-point VSC-HVDC configuration system. In this scheme, the DC link is used to transmit the bulk power between converters, which are at different locations.[6,13,14]

Although most of these VSC-HVDC interconnections are 2-terminal, their modus operandi can also be extended to multiterminal HVDC (MTDC) systems.

Unlike the 2-terminal HVDC interconnection, the MTDC system is more versatile and better capable to use the economic and technical advantages of the VSC-HVDC technology. It is also better suited if futuristic integration of renewable energy sources are planned.[13,14]

Many recent works have been done in the VSC-HVDC system based on multilevel converters,[15–19] which have well-known attractive features in high-voltage and high-power applications.[15–18]

Indeed, multilevel converters have shown some significant advantages over traditional 2-level converters. They provide higher power quality at the AC side, can operate at higher AC voltage levels and minimize or even eliminate the interface transformer and reduce switching losses.[19–21] Generally, multilevel VSC can be divided into various topologies such as neutral point clamped (NPC), flying capacitor Cascade H-Bridge, and modular multilevel converters (MMC).[22–25] Recently, a new topology called T-type was proposed as a potential alternative to NPC structure. This converter merges the merit to operate at reduced conduction losses and the well-known advantages of multilevel converters.[24,26,27] Compared to the NPC and MMC topologies, T-type topology presents fewer semiconductors, which leads to a cost-effective multilevel structure.[28] In addition, its modulation techniques are simpler compared to the MMC topology. However, the DC bus capacitors voltage balancing problem has been recognized as the major limitation of this kind of multilevel converter. Several techniques have been already proposed to achieve voltage balancing in multilevel converters. One category of these techniques suggests the use of auxiliary power circuits.[11] However, this solution increases the cost and the complexity of the converter. To overcome the drawbacks of the hardware solution, an interesting solution based on multilevel space vector modulated (SVM) is proposed in the previous studies.[19–21] In this approach, the multilevel SVM algorithm is equipped by a balancing strategy based on the effective use of the redundant switching states of the converters voltage vectors.

Various control strategies have been proposed to control the HVDC system.[19,29] One of these strategies is the direct power control (DPC). The basic idea of the classical DPC is the direct control of active and reactive power without any internal control loop or Pulse Width Modulation (PWM) modulator.[30,31] The switching states are selected via a switching table, and the states are chosen on the basis of the instantaneous error between the estimated and the desired active and reactive power. Simple structure and very good dynamic behavior are main features of classical DPC.[30,31] However, the main disadvantages of the classical DPC are the variable switching frequency and lack of fast current regulation, which increases the risk of device failure during faults. The DPC can be forced to operate at a constant frequency by substituting the switching table by an SVM.[21,32] On the other hand, AC-line voltage sensor can be replaced by a virtual flux (VF) estimator to establish the so-called VF-DPC-SVM, which brings benefits such as simplification and isolation between the power circuit and control system.[21,33]

In this study, a nonlinear control strategy based on backstepping controller associated to VF-DPC-SVM is applied to a 5-level T-type MTDC transmission system. The control objectives are (1) controlling the active and reactive power of the network sides, (2) generating sinusoidal currents in the AC sides of converters, and (3) regulating the DC bus voltage between the terminals of the MTDC system.

The rest of the paper is organized as follows. In Section 2, a mathematical model of the MTDC system based on T-type converters is presented. In this section, the principle of operation of 5-level T-type converter, the SVM-based switching strategy, and the DC capacitor voltage balancing method are detailed. In Section 3, nonlinear control for MTDC system based on backstepping method is developed. Simulation results are presented and illustrated in Section 4. At last, conclusions are drawn in Section 5.

## 2 | MTDC SYSTEM STUDY AND MODELING

Figure 1 shows a schematic representation of an MTDC transmission system. MTDC is composed of 2 parts: OWFs sides and grid side. At the OWFs side, a 5-level rectifier is used to perform AC to DC conversion. A DC cable is used to join the terminals to the sending end. Each DC transmission line is modeled by 2 T-sections.

Electricity will be transferred through DC cables to the receiving end point, and finally reaching inverter terminal.

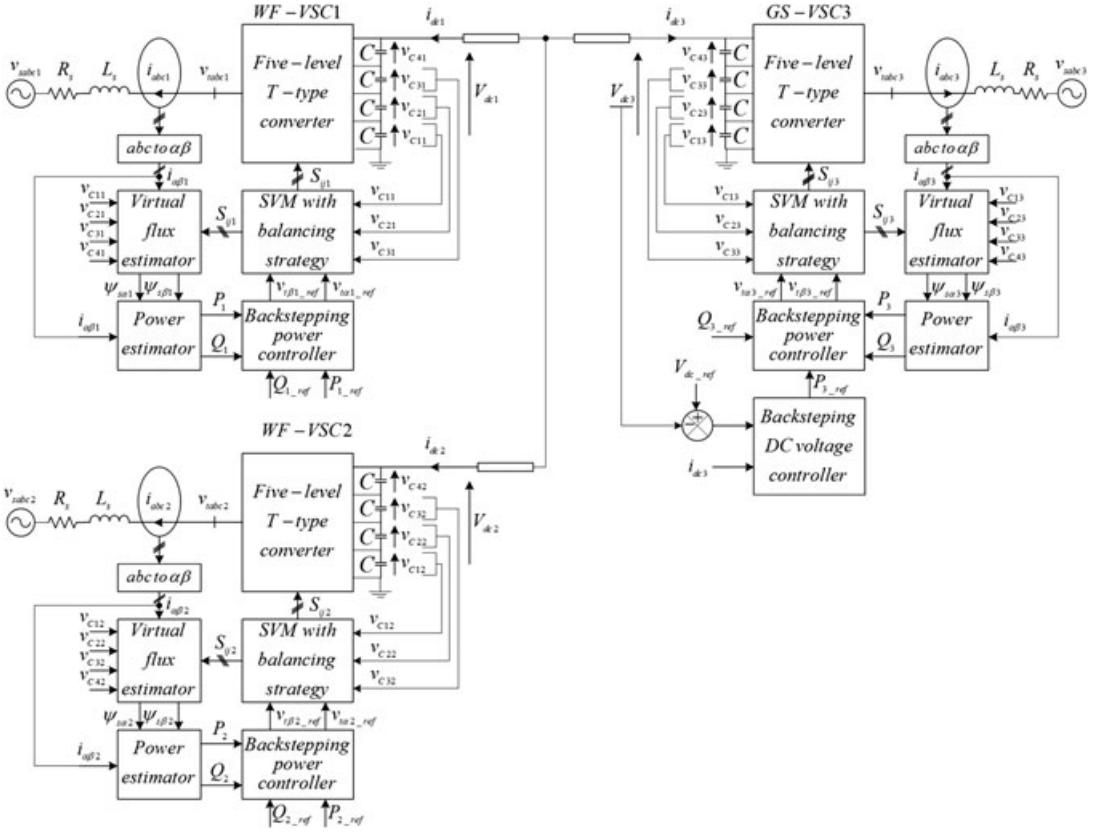


**FIGURE 1** A schematic representation of virtual flux direct power-backstepping control of 5-level T-type multiterminal voltage source converter high-voltage direct current system

At the 5-level inverter terminal, electricity will be converted again from DC back to AC.

The presence of the reactance $L_s$ and $R_s$ in AC sides of both OWFs and grid, and the use of 5-level SVM to control the 5-level converters, help to stabilize the AC currents and reduce the currents harmonics.

To avoid repetition in the problem formulation, the quantities of OWF-VSC1 and AC system-1 are indexed by k = 1, and OWF-VSC2 and AC system-2 are indexed by k = 2, while those of GS-VSC3 and AC system-3 are indexed by k = 3.

## 2.1 | Modeling and analysis of the 5-level T-type converter

The basic topology of the 5-level T-type converter is depicted in Figure 2.

Five-level T-type topology is composed by dual 3-level T-type modules. Each leg consists of eight insulated gate bipolar transistors with antiparallel diodes and 2 clamping diodes. These switches operate in switch pairs $\left(S_{ijk}, \overline{S}_{ijk}\right), i = a, b, c,\ j = 1, 2, 3, 4$and in a complementary manner. Among the 8 active devices in a converter leg, only 2 devices are involved in the transition between the adjacent states.

As shown in Table 1, five different output voltage levels can be synthesized according to their switching states.

The expressions of instantaneous converters phase voltages are given by

$$\begin{bmatrix} v_{tak} \\ v_{tbk} \\ v_{tck} \end{bmatrix} = \frac{1}{3} \begin{bmatrix} \sum_{j=1}^{4} \left( \left(2F_{ajk} - F_{bjk} - F_{cjk}\right) \sum_{i=1}^{j} v_{Cik} \right) \\ \sum_{j=1}^{4} \left( \left(2F_{bjk} - F_{ajk} - F_{cjk}\right) \sum_{i=1}^{j} v_{Cik} \right) \\ \sum_{j=1}^{4} \left( \left(2F_{cjk} - F_{ajk} - F_{bjk}\right) \sum_{i=1}^{j} v_{Cik} \right) \end{bmatrix}, \quad (1)$$

where $v_{txk},\ x = a, b, c$ are the output voltages of the T-type converter and $v_{Cik},\ i = 1, 2, 3, 4$ are the voltages of $C_{ik}$ capacitors. The output voltages are expressed using the switching functions of the 5-level T-type converter as follows:

$$\begin{aligned} F_{x4k} &= S_{x4k}S_{x3k}S_{x2k}S_{x1k} \\ F_{x3k} &= S_{x4k}S_{x3k}S_{x2k}\overline{S}_{x1k} \\ F_{x2k} &= S_{x4k}S_{x3k}\overline{S}_{x2k}\overline{S}_{x1k} \\ F_{x1k} &= S_{x4k}\overline{S}_{x3k}\overline{S}_{x2k}\overline{S}_{x1k} \end{aligned} \qquad x = a, b, c. \quad (2)$$

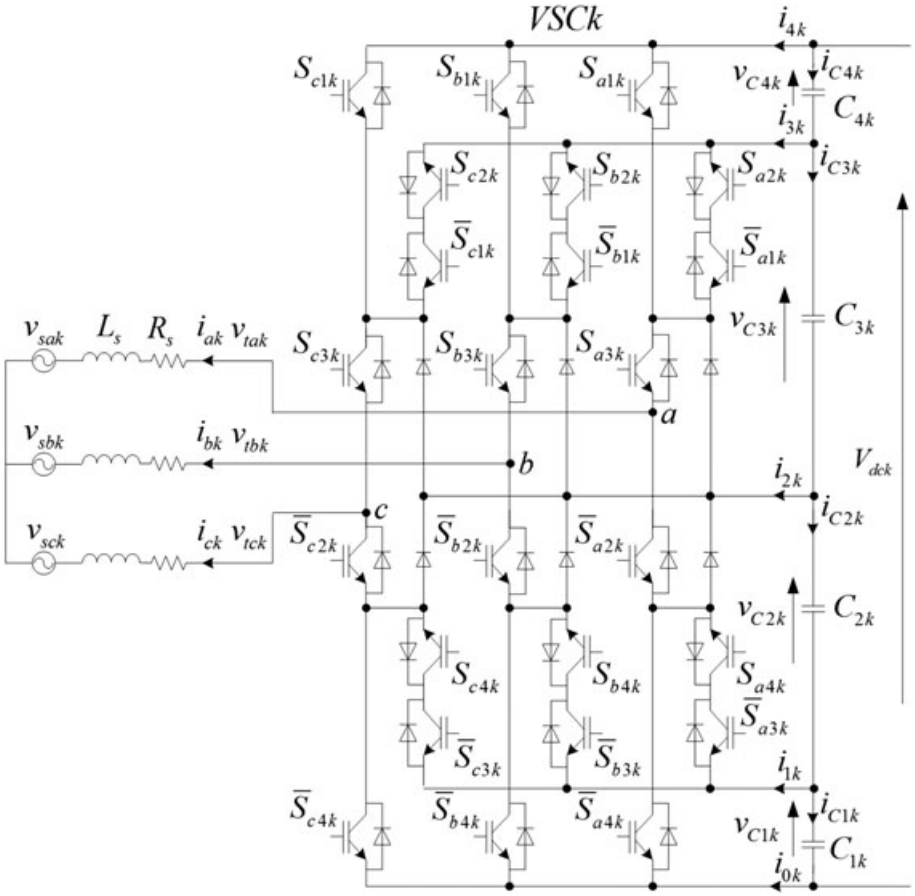


**FIGURE 2** A basic topology of the 5-level T-type converter

**TABLE 1** Definition of switching states

| $S_{i1k}$ | $S_{i2k}$ | $S_{i3k}$ | $S_{i4k}$ | $\overline{S}_{i1k}$ | $\overline{S}_{i2k}$ | $\overline{S}_{i3k}$ | $\overline{S}_{i4k}$ | $v_{i0k}$ |
|---|---|---|---|---|---|---|---|---|
| 1 | 1 | 1 | 1 | 0 | 0 | 0 | 0 | $v_{C3k}+v_{C4k}$ |
| 0 | 1 | 1 | 1 | 1 | 0 | 0 | 0 | $v_{C3k}$ |
| 0 | 0 | 1 | 1 | 1 | 1 | 0 | 0 | 0 |
| 0 | 0 | 0 | 1 | 1 | 1 | 1 | 0 | $-v_{C2k}$ |
| 0 | 0 | 0 | 0 | 1 | 1 | 1 | 1 | $-(v_{C1k}+v_{C2k})$ |

For each terminal station, the dynamic equations of AC side are expressed as

$$\frac{di_{xk}}{dt}=\frac{1}{L_s}(v_{txk}-v_{sxk}-R_s i_{xk}),\quad x=a,b,c, \tag{3}$$

where $i_{xk}$ are the line currents, $v_{sxk}$ are the source voltages, and $R_s$ and $L_s$ represent series-connected phase reactors.

To make the model in a more simplified form, the Concordia transformation is applied in Equation 3, which gives

$$\begin{cases}\dfrac{d\,i_{\alpha k}}{dt}=\dfrac{1}{L_s}(v_{t\alpha k}-v_{s\alpha k}-R_s\,i_{\alpha k})\\ \dfrac{d\,i_{\beta k}}{dt}=\dfrac{1}{L_s}(v_{t\beta k}-v_{s\beta k}-R_s\,i_{\beta k})\end{cases}, \tag{4}$$

where $v_{s\alpha k}$ and $v_{s\beta k}$ are the $\alpha\beta$ axes components of the respective source voltages, $i_{\alpha k}$ and $i_{\beta k}$ are the line current components, and $v_{t\alpha k}$ and $v_{t\alpha k}$ are the converter output voltage components.

On the other hand, the DC side is governed by

$$\frac{dV_{dck}}{dt}=\frac{i_{dck}}{C_{eqk}}-\frac{P_k}{C_{eqk}V_{dck}}, \tag{5}$$

where $V_{dck}$ is the DC bus voltage, $i_{dck}$ is the current of the line transmission, $P_k$ is the power of DC-side, and $C_{eq}=C_{ik}/4,\quad i=1,2,3,4$ is the DC-link equivalent capacitor.

## 2.2 | Five-level space vector modulation

### 2.2.1 | Determination of the space vector location

The space vector location is fulfilled in 2 steps. The first step determines the sector number of where the reference voltage vector lies. The second step is dedicated to the computation of the triangle number in which the reference voltage vector is located.[34]

Step 1. Sector number computation

The module and the position of the reference voltage vector are determined from

$$\begin{aligned} v_{tk_{ref}} &= \sqrt{v_{t\alpha k_{ref}}^2 + v_{t\alpha k_{ref}}^2} \\ \theta_k &= \tan 2^{-1}\left(\frac{v_{t\beta k_{ref}}}{v_{t\alpha k_{ref}}}\right), \end{aligned} \tag{6}$$

where $\tan 2^{-1}$ is the C-function, which returns the inverse tangent in the 4 quadrants of the unit circle. Once the value of $\theta_k$ is calculated, the numbers of sectors are given by

$$S_k = ceil\left(\frac{\theta_k}{\pi/3}\right) \in \{1,\ 2,\ 3,\ 4,\ 5,\ 6\}, \tag{7}$$

Where *ceil* is the C-function that returns the smallest integer value greater than or equal to the argument passed to it.

Step 2. Triangle identification

For triangle identification, reference vector $v_{tk\_ref}$ is projected on the axes of 60° coordinate system.[21] The projected components are $v_{1ref}^{S_k}$ and $v_{2ref}^{S_k}$, which are expressed by

$$\begin{aligned} v_{1_{ref}}^{S_k} &= 4m\left(\cos\left(\theta_k - (S_k-1)\frac{\pi}{3}\right) - \frac{1}{\sqrt{3}}\sin\left(\theta_k - (S_k-1)\frac{\pi}{3}\right)\right) \\ v_{2_{ref}}^{S_k} &= 4m\left(\frac{2}{\sqrt{3}}\sin\left(\theta_k - (S_k-1)\frac{\pi}{3}\right)\right), \end{aligned} \tag{8}$$

where the modulation rate $m$ is given by

$$m = \frac{v_{tk_{ref}}}{\sqrt{2/3}V_{dck}}. \tag{9}$$

Figure 3 presents $v_{tk\_ref}$ project in the first sector. To identify the triangle where the required reference is located, the following integers are used:

$$\begin{aligned} l_1^{S_k} &= \text{int}\left(v_{1_{ref}}^{S_k}\right) \\ l_2^{S_k} &= \text{int}\left(v_{2_{ref}}^{S_k}\right), \end{aligned} \tag{10}$$

where int() is a C-function giving the integer part of a given real number.

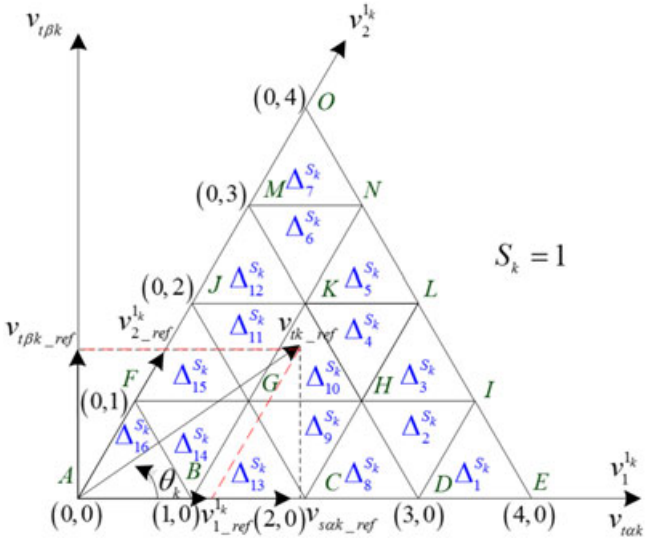


**FIGURE 3** Reference voltages project in the first sector

The triangle number is obtained according to the value of $l_1^{S_k}$ and $l_2^{S_k}$, as shown in Table 2.

### 2.2.2 | Duration time calculation

The average value of the reference voltage vector is synthesized by averaging the 3 adjacent voltage vectors according to the following equation:

$$\frac{1}{T_c}\int_t^{t+T_c} v_{tk_{ref}}\,dt = \frac{1}{T_c}\left(\int_t^{t+t_x^{\Delta_i^{S_k}}} v_x^{\Delta_i^{S_k}}\,dt + \int_{t+t_x^{\Delta_i^{S_k}}}^{t+t_x^{\Delta_i^{S_k}}+t_y^{\Delta_i^{S_k}}} v_y^{\Delta_i^{S_k}}\,dt + \int_{t+t_x^{\Delta_i^{S_k}}+t_y^{\Delta_i^{S_k}}}^{t+T_c} v_z^{\Delta_i^{S_k}}\,dt\right), \tag{11}$$

where $t_x^{\Delta_i^{S_k}}$, $t_y^{\Delta_i^{S_k}}$ and $t_z^{\Delta_i^{S_k}}$ are the application time of the adjacent vectors $v_x^{\Delta_i^{S_k}}$, $v_y^{\Delta_i^{S_k}}$ and $v_z^{\Delta_i^{S_k}}$, respectively.

During a small switching cycle $T_c$, the voltage vectors can be assumed constant, which leads to

$$\begin{aligned} v_x^{\Delta_i^{S_k}} t_x^{\Delta_i^{S_k}} + v_y^{\Delta_i^{S_k}} t_y^{\Delta_i^{S_k}} + v_z^{\Delta_i^{S_k}} t_z^{\Delta_i^{S_k}} &= v_{tk_{ref}} T_c \\ t_x^{\Delta_i^{S_k}} + t_y^{\Delta_i^{S_k}} + t_z^{\Delta_i^{S_k}} &= T_c. \end{aligned} \tag{12}$$

The projection of Equation 12 in the coordinate system formed by the 2 axes making 60° between them results in

$$\begin{aligned} v_{x1}^{\Delta_i^{S_k}} t_x^{\Delta_i^{S_k}} + v_{y1}^{\Delta_i^{S_k}} t_y^{\Delta_i^{S_k}} + v_{z1}^{\Delta_i^{S_k}} t_z^{\Delta_i^{S_k}} &= v_{1_{ref}}^{S_k} T_c \\ v_{x2}^{\Delta_i^{S_k}} t_x^{\Delta_i^{S_k}} + v_{y2}^{\Delta_i^{S_k}} t_y^{\Delta_i^{S_k}} + v_{z2}^{\Delta_i^{S_k}} t_z^{\Delta_i^{S_k}} &= v_{2_{ref}}^{S_k} T_c \\ t_x^{\Delta_i^{S_k}} + t_y^{\Delta_i^{S_k}} + t_z^{\Delta_i^{S_k}} &= T_c. \end{aligned} \tag{13}$$

**TABLE 2** Triangle identification

| $\Delta_i^{S_k}$ | Condition of triangle identification |
|---|---|
| $\Delta_{16}^{S_k}$ | $v_{1ref}^{S_k}<1,\ v_{2ref}^{S_k}<1$ and $v_{1ref}^{S_k}+v_{2ref}^{S_k}<1$ |
| $\Delta_{14}^{S_k}$ | $v_{1ref}^{S_k}<1,\ v_{2ref}^{S_k}<1$ and $v_{1ref}^{S_k}+v_{2ref}^{S_k}\geq 1$ |
| $\Delta_{13}^{S_k}$ | $v_{1ref}^{S_k}<2,\ v_{2ref}^{S_k}<1$ and $v_{1ref}^{S_k}+v_{2ref}^{S_k}<2$ |
| $\Delta_{9}^{S_k}$ | $v_{1ref}^{S_k}<2,\ v_{2ref}^{S_k}<1$ and $v_{1ref}^{S_k}+v_{2ref}^{S_k}\geq 2$ |
| $\Delta_{8}^{S_k}$ | $v_{1ref}^{S_k}<3,\ v_{2ref}^{S_k}<1$ and $v_{1ref}^{S_k}+v_{2ref}^{S_k}<3$ |
| $\Delta_{2}^{S_k}$ | $v_{1ref}^{S_k}<3,\ v_{2ref}^{S_k}<1$ and $v_{1ref}^{S_k}+v_{2ref}^{S_k}\geq 3$ |
| $\Delta_{1}^{S_k}$ | $v_{1ref}^{S_k}<4,\ v_{2ref}^{S_k}<1$ |
| $\Delta_{15}^{S_k}$ | $v_{1ref}^{S_k}<1,\ v_{2ref}^{S_k}<2$ and $v_{1ref}^{S_k}+v_{2ref}^{S_k}<2$ |
| $\Delta_{11}^{S_k}$ | $v_{1ref}^{S_k}<1,\ v_{2ref}^{S_k}<2$ and $v_{1ref}^{S_k}+v_{2ref}^{S_k}\geq 2$ |
| $\Delta_{10}^{S_k}$ | $v_{1ref}^{S_k}<2,\ v_{2ref}^{S_k}<2$ and $v_{1ref}^{S_k}+v_{2ref}^{S_k}<3$ |
| $\Delta_{4}^{S_k}$ | $v_{1ref}^{S_k}<2,\ v_{2ref}^{S_k}<2$ and $v_{1ref}^{S_k}+v_{2ref}^{S_k}\geq 3$ |
| $\Delta_{3}^{S_k}$ | $v_{1ref}^{S_k}<3,\ v_{2ref}^{S_k}<2$ |
| $\Delta_{12}^{S_k}$ | $v_{1ref}^{S_k}<1,\ v_{2ref}^{S_k}<3$ and $v_{1ref}^{S_k}+v_{2ref}^{S_k}<3$ |
| $\Delta_{6}^{S_k}$ | $v_{1ref}^{S_k}<1,\ v_{2ref}^{S_k}<3$ and $v_{1ref}^{S_k}+v_{2ref}^{S_k}\geq 3$ |
| $\Delta_{5}^{S_k}$ | $v_{1ref}^{S_k}<2,\ v_{2ref}^{S_k}<3$ |
| $\Delta_{7}^{S_k}$ | $v_{1ref}^{S_k}<1,\ v_{2ref}^{S_k}<4$ |

The calculation of $t_x^{\Delta_i^{S_k}}$, $t_y^{\Delta_i^{S_k}}$ and $t_z^{\Delta_i^{S_k}}$ requires the substitution of the coordinates of $v_x^{\Delta_i^{S_k}}$, $v_y^{\Delta_i^{S_k}}$ and $v_z^{\Delta_i^{S_k}}$ vectors. The on-duration time intervals are summarized in Table 3.

## 2.3 | DC-capacitor voltages balancing strategy

In this section, minimum energy property is used to avoid voltage drift phenomenon. Assuming that all the capacitors have equal capacitance $C_{1k}=C_{2k}=C_{3k}=C_{4k}=C$, the total energy of 4 capacitors is given by

$$E_k=\frac{C}{2}\sum_{i=1}^{4}v_{Cik}^2. \tag{14}$$

When all capacitors voltages are balanced, $E_k$ reaches the following minimum value:

$$E_{k\min}=\frac{1}{2}C\frac{V_{dck}^2}{4}. \tag{15}$$

To reduce the gap between each DC voltage and its reference value, a cost function $J_k$ is defined. This function is based on the sum of the squared differences between the capacitor voltages and their reference values.

**TABLE 3** Duration time calculation

| $\Delta_i^{S_k}(x,y,z)$ | $t_x^{\Delta_i^{S_k}}$ | $t_y^{\Delta_i^{S_k}}$ | $t_z^{\Delta_i^{S_k}}$ |
|---|---|---|---|
| $\Delta_1^{S_k}(D,E,I)$ | $T_c-t_y^{\Delta_1^{S_k}}-t_z^{\Delta_1^{S_k}}$ | $\left(v_{1ref}^{S_k}-3\right)T_c$ | $v_{2ref}^{S_k}T_c$ |
| $\Delta_2^{S_k}(I,H,D)$ | $T_c-t_y^{\Delta_2^{S_k}}-t_z^{\Delta_2^{S_k}}$ | $\left(3-v_{1ref}^{S_k}\right)T_c$ | $\left(1-v_{2ref}^{S_k}\right)T_c$ |
| $\Delta_3^{S_k}(H,I,L)$ | $T_c-t_y^{\Delta_3^{S_k}}-t_z^{\Delta_3^{S_k}}$ | $\left(v_{1ref}^{S_k}-2\right)T_c$ | $\left(v_{2ref}^{S_k}-1\right)T_c$ |
| $\Delta_4^{S_k}(L,K,H)$ | $T_c-t_y^{\Delta_4^{S_k}}-t_z^{\Delta_4^{S_k}}$ | $\left(2-v_{1ref}^{S_k}\right)T_c$ | $\left(2-v_{2ref}^{S_k}\right)T_c$ |
| $\Delta_5^{S_k}(K,L,N)$ | $T_c-t_y^{\Delta_5^{S_k}}-t_z^{\Delta_5^{S_k}}$ | $\left(v_{1ref}^{S_k}-1\right)T_c$ | $\left(v_{2ref}^{S_k}-2\right)T_c$ |
| $\Delta_6^{S_k}(N,M,K)$ | $T_c-t_y^{\Delta_6^{S_k}}-t_z^{\Delta_6^{S_k}}$ | $\left(1-v_{1ref}^{S_k}\right)T_c$ | $\left(3-v_{2ref}^{S_k}\right)T_c$ |
| $\Delta_7^{S_k}(M,N,O)$ | $T_c-t_y^{\Delta_7^{S_k}}-t_z^{\Delta_7^{S_k}}$ | $v_{1ref}^{S_k}T_c$ | $\left(v_{2ref}^{S_k}-3\right)T_c$ |
| $\Delta_8^{S_k}(C,D,H)$ | $T_c-t_y^{\Delta_8^{S_k}}-t_z^{\Delta_8^{S_k}}$ | $\left(v_{1ref}^{S_k}-2\right)T_c$ | $v_{2ref}^{S_k}T_c$ |
| $\Delta_9^{S_k}(H,G,C)$ | $T_c-t_y^{\Delta_9^{S_k}}-t_z^{\Delta_9^{S_k}}$ | $\left(2-v_{1ref}^{S_k}\right)T_c$ | $\left(1-v_{2ref}^{S_k}\right)T_c$ |
| $\Delta_{10}^{S_k}(G,H,K)$ | $T_c-t_y^{\Delta_{10}^{S_k}}-t_z^{\Delta_{10}^{S_k}}$ | $\left(v_{1ref}^{S_k}-1\right)T_c$ | $\left(v_{2ref}^{S_k}-1\right)T_c$ |
| $\Delta_{11}^{S_k}(K,J,G)$ | $T_c-t_y^{\Delta_{11}^{S_k}}-t_z^{\Delta_{11}^{S_k}}$ | $\left(1-v_{1ref}^{S_k}\right)T_c$ | $\left(2-v_{2ref}^{S_k}\right)T_c$ |
| $\Delta_{12}^{S_k}(J,K,M)$ | $T_c-t_y^{\Delta_{12}^{S_k}}-t_z^{\Delta_{12}^{S_k}}$ | $v_{1ref}^{S_k}T_c$ | $\left(v_{2ref}^{S_k}-2\right)T_c$ |
| $\Delta_{13}^{S_k}(B,C,J)$ | $T_c-t_y^{\Delta_{13}^{S_k}}-t_z^{\Delta_{13}^{S_k}}$ | $\left(v_{1ref}^{S_k}-1\right)T_c$ | $v_{2ref}^{S_k}T_c$ |
| $\Delta_{14}^{S_k}(G,F,B)$ | $T_c-t_y^{\Delta_{14}^{S_k}}-t_z^{\Delta_{14}^{S_k}}$ | $\left(1-v_{1ref}^{S_k}\right)T_c$ | $\left(1-v_{2ref}^{S_k}\right)T_c$ |
| $\Delta_{15}^{S_k}(F,G,J)$ | $T_c-t_y^{\Delta_{15}^{S_k}}-t_z^{\Delta_{15}^{S_k}}$ | $v_{1ref}^{S_k}T_c$ | $\left(v_{2ref}^{S_k}-1\right)T_c$ |
| $\Delta_{16}^{S_k}(A,B,F)$ | $T_c-t_y^{\Delta_{16}^{S_k}}-t_z^{\Delta_{16}^{S_k}}$ | $v_{1ref}^{S_k}T_c$ | $v_{2ref}^{S_k}T_c$ |

$$J_k=\frac{1}{2}C\sum_{i=1}^{4}\left(v_{Cik}-\frac{V_{dck}}{4}\right)^2 \tag{16}$$

Based on a suitable choice of the redundant vectors, the cost function $J_k$ can be minimized to zero. Consequently,

**TABLE 4** Simulation parameters

| Parameter | Value |
|---|---|
| Source voltage $v_{sk\_abc}$ | *25 kV* |
| Frequencies of the grids $f_1, f_2, f_3$ | *60 Hz,60 Hz,50 Hz* |
| Line impedance $R_s, L_s$ | *0.04 Ω, 0.006 H* |
| DC-link capacitance $C_{kj}$ | *1mF* |

**TABLE 5** Simulation conditions

| Time, s | 0-0.3 | 0.3-0.5 | 0.5-0.7 | 0.7-1 |
|---|---|---|---|---|
| $P_{1\_ref}$ | *−100 MW* | *−85 MW* | *−85 MW* | *−100 MW* |
| $P_{2\_ref}$ | *−85 MW* | *−85 MW* | *−100 MW* | *−100 MW* |

the capacitor voltages will be maintained at their reference values, and $E_k$ will be reduced to $E_{k\min}$. The mathematical condition ensuring the convergence of the cost function $J_k$ to its minimum value is given by

$$\frac{dJ_k}{dt} = C\sum_{i=1}^{4}\Delta v_{Cik}\frac{dv_{Cik}}{dt} = \sum_{i=1}^{4}\Delta v_{Cik}i_{Cik} \leq 0, \tag{17}$$

where $\Delta v_{Cik} = v_{Cik} - (V_{dck}/4)$ is the error voltage of the capacitor $C_{ik}$. Note that the currents of capacitors $i_{C1k}, i_{C2k}, i_{C3k}$, and $i_{C4k}$ are affected by the intermediate input DC currents $i_{3k}^{S_k}, i_{2k}^{S_k}$ and $i_{1k}^{S_k}$. On the other hand, as the input current can be calculated from the switching vectors and their application time, it is advantageous to express the Equation 17 on the basis of the current $i_{3k}^{S_k}, i_{2k}^{S_k}$ and $i_{1k}^{S_k}$.[19,20] Indeed, the DC-capacitor currents are expressed as

$$i_{Cik} = \frac{1}{4}\sum_{j=1}^{3}x_k i_{jk}^{S_k} - \sum_{j=i}^{3}i_{jk}^{S_k}, \qquad i = 1,2,3,4. \tag{18}$$

If the total DC voltage is kept at a constant value, it results in

$$\sum_{i=1}^{4}\Delta v_{Cik} = 0. \tag{19}$$

By substituting for $i_{Cik}$ from Equation 18 and $\Delta v_{C4k}$ from Equation 19, the balancing condition can be reduced to

$$\sum_{i=1}^{3}\Delta v_{Cik}\left(\sum_{j=i}^{3}i_{jk}^{S_k}\right) \geq 0. \tag{20}$$

The application of the mean operator in Equation 20 during a switching period $T_c$ gives

$$\frac{1}{T_c}\int_{KT_c}^{(K+1)T_c}\left[\sum_{i=1}^{3}\Delta v_{Cik}\left(\sum_{j=i}^{3}i_{jk}^{S_k}\right)\right]dt \geq 0. \tag{21}$$

Assuming that the switching period is small compared to the response time of the capacitor voltages, capacitors voltages can be considered as constants,[19,20] and therefore, Equation 21 can be simplified to

$$\sum_{i=1}^{3}\Delta v_{Cik}(K)\left(\sum_{j=i}^{3}\bar{i}_{jk}^{S_k}(K)\right) \geq 0, \tag{22}$$

where $\Delta v_{Cik}(K)$ is the voltage error of capacitor $C_{ik}$ at sampling period $(K)$ and $\bar{i}_{jk}^{S_k}(K)$ is the mean value of the input current $i_{jk}$.

When the tip of reference voltage vector $v_{tk\_ref}$ is located in sector $S_k = 1$, the average values of the DC-side intermediate branch currents are

$$\begin{bmatrix}\bar{i}_{3k}^{S_k}\\ \bar{i}_{2k}^{S_k}\\ \bar{i}_{1k}^{S_k}\end{bmatrix} = \frac{1}{T_s}\begin{bmatrix}i_{3xk}^{S_k} & i_{3yk}^{S_k} & i_{3zk}^{S_k}\\ i_{2xk}^{S_k} & i_{2yk}^{S_k} & i_{2zk}^{S_k}\\ i_{1xk}^{S_k} & i_{1yk}^{S_k} & i_{1zk}^{S_k}\end{bmatrix}\begin{bmatrix}t_x^{\Delta_i^{S_k}}\\ t_y^{\Delta_i^{S_k}}\\ t_z^{\Delta_i^{S_k}}\end{bmatrix}, \tag{23}$$

where $i_{jxk}^{S_k}$, $i_{jyk}^{S_k}$ and $i_{jzk}^{S_k}$, $(j = 1,\ 2,\ 3)$ are the charging currents for switching states $x$, $y$, and $z$ in the triangle $\Delta_i^{S_k}$ minimizing the cost function $J_k$.

## 3 | VIRTUAL FLUX DIRECT POWER-BACKSTEPPING CONTROL

In this section, direct power-backstepping control with space vector modulation based on the concept of VF is investigated. The backstepping VF-DPC-SVM control strategy main scheme is presented in Figure 1.

### 3.1 | Virtual flux estimator

The concept of the VF for power estimation is introduced by Malinowksi.[33] The principle of VF is based on a duality with the PWM converter fed induction motor, where $R_s$ and $L_s$ represent the stator resistance and leakage inductance of the

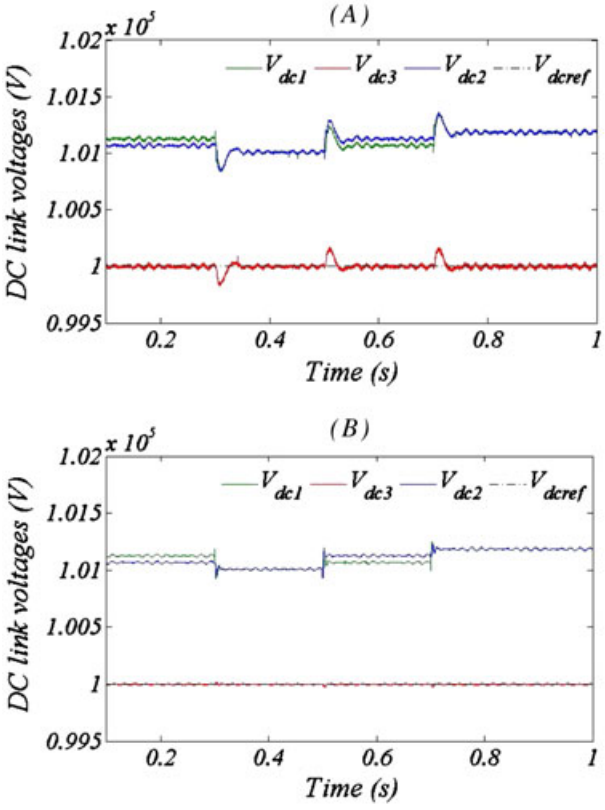


**FIGURE 4** Simulation results of DC-links voltages: (A) with PI control, (B) with backstepping control

virtual motor.[33] Based on this approach, VF components can be estimated by

$$\begin{aligned} \psi_{s\alpha k} &= \int v_{s\alpha k} dt \\ \psi_{s\beta k} &= \int v_{s\beta k} dt. \end{aligned} \tag{24}$$

The voltages $v_{s\alpha k}$ and $v_{s\beta k}$ are estimated by the following equation

$$\begin{aligned} v_{s\alpha k} &= v_{t\alpha k} - L_s \frac{di_{\alpha k}}{dt} \\ v_{s\beta k} &= v_{t\beta k} - L_s \frac{di_{\beta k}}{dt}. \end{aligned} \tag{25}$$

The integration of both sides of Equation 25 gives

$$\begin{aligned} \psi_{s\alpha k} &= \int v_{t\alpha k} dt - L_s i_{\alpha k} \\ \psi_{s\beta k} &= \int v_{t\beta k} dt - L_s i_{\beta k}. \end{aligned} \tag{26}$$

## 3.2 | Active and reactive power estimator

The estimated active and reactive power can be described by the following formulas:

$$\begin{aligned} P_k &= \omega_k \left( \psi_{s\alpha k} i_{\beta k} - \psi_{s\beta k} i_{\alpha k} \right) \\ Q_k &= \omega_k \left( \psi_{s\alpha k} i_{\alpha k} + \psi_{s\beta k} i_{\beta k} \right), \end{aligned} \tag{27}$$

where $\omega_k$ is the angular frequency of the network $k$.

## 3.3 | Backstepping control design

In the MTDC system, the inverters stations are charged to control both the active and reactive power exchanges between the AC systems and DC links. At the same time, the rectifier station controls the DC voltage and the reactive power, where the reference value of the active power is delivered by the DC voltage controller.

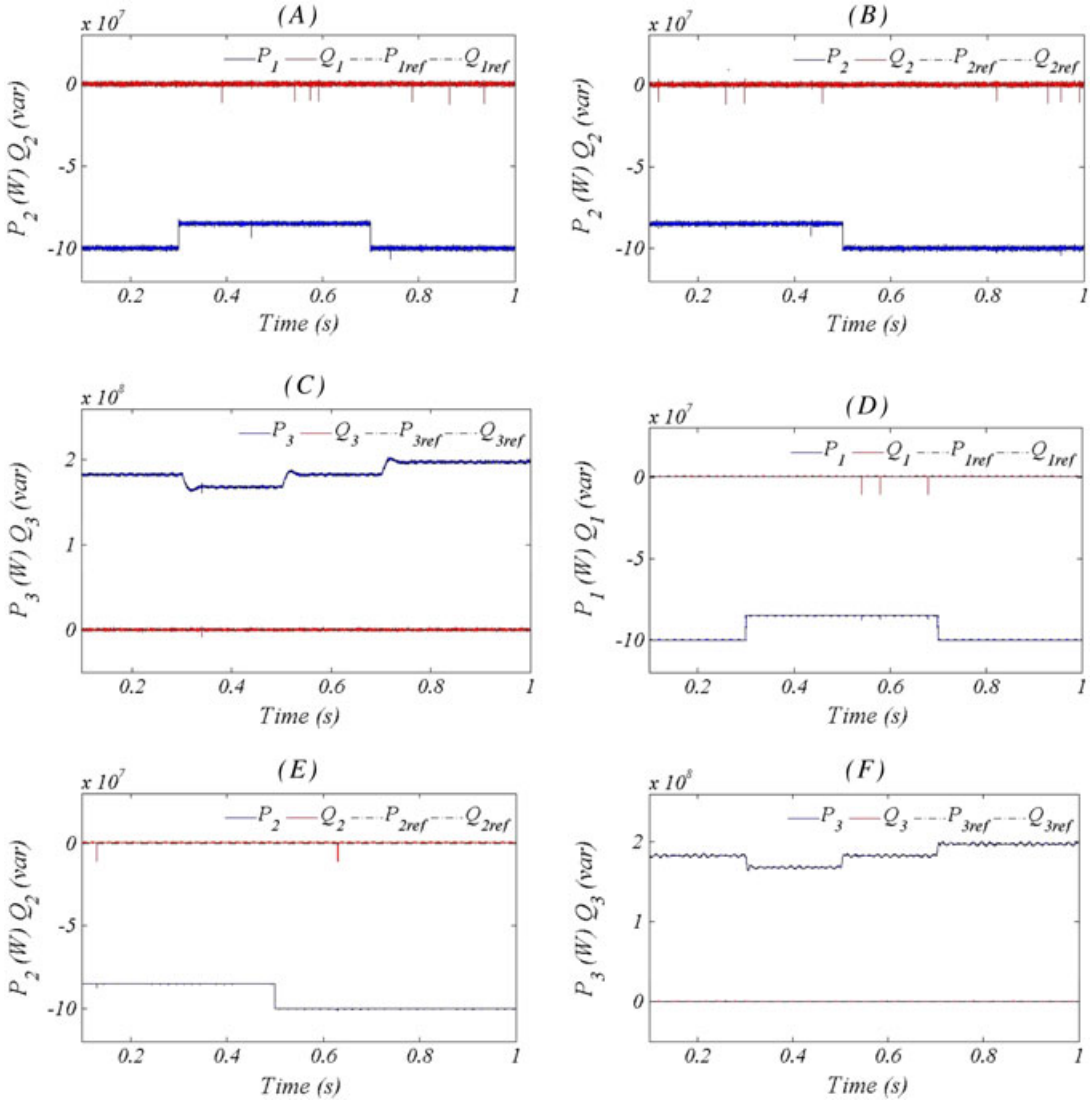


**FIGURE 5** Simulation results of active and reactive power: (A,B,C) with PI control, (D,E,F) with backstepping control

To make the application of nonlinear control possible, the approach adopted herein is based on breaking down a complex nonlinear system into smaller subsystems, and then the control law is designed for each subsystem.[21] To design the control algorithm for MTDC system with the aid of backstepping method, the system model is portioned in 3 single-input single-output subsystems in the following form:

$$\begin{aligned} \dot{\zeta}_{nk} &= L_{f_{nk}} h_{nk} + L_{g_{nk}} h_{nk} u_{nk} \\ y_{nk} &= h_{nk}(\zeta_{nk}); \;\; n = 1, 2, 3, \end{aligned} \tag{28}$$

where $\zeta_{nk}, u_{nk}$ and $y_{nk}$ represent state, control input, and output of $n^{th}$ subsystem, respectively. $f_{nk}$ and $g_{nk}$ are smooth fields, and $h_{nk}$ is a smooth scalar function. The term $L_{f_{nk}} h_{nk}$ stands for the Lie derivative of $h_{nk}$ with respect to $f_{nk}$, similarly with $L_{g_{nk}} h_{nk}$.

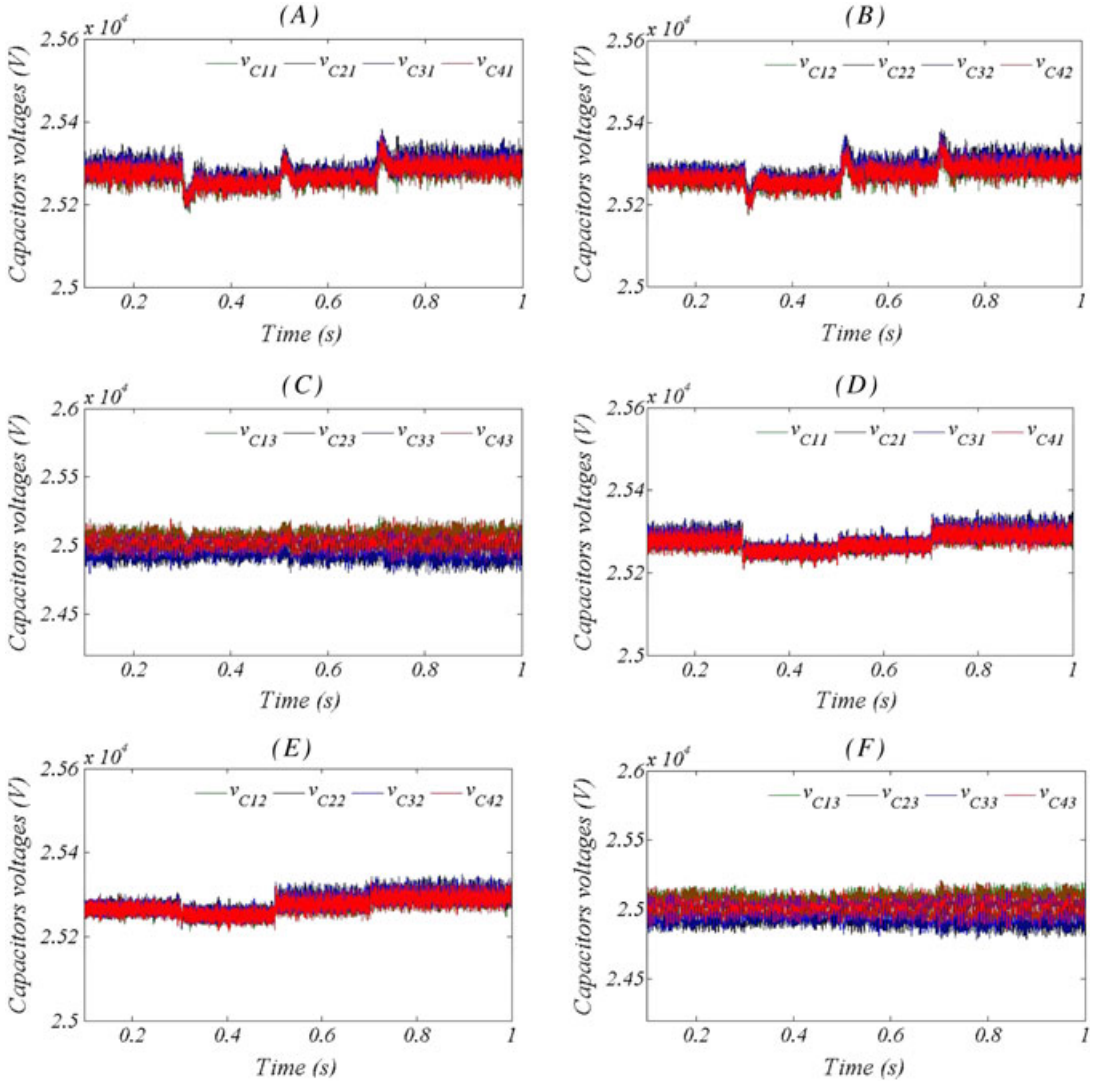


**FIGURE 6** Simulation results of DC capacitors voltages: (A,B,C) with PI control, (D,E,F) with backstepping control

**TABLE 6** Harmonic spectrum of line currents

| | OWF-VSC1 (60 Hz) | OWF-VSC2 (60 Hz) | GS-VSC3 (50 Hz) |
|---|---|---|---|
| PI control | Fundamental = 2473 A<br>THD = 1.35% | Fundamental = 2474 A<br>THD = 1.34% | Fundamental = 4832 A<br>THD = 0.96% |
| Backstepping control | Fundamental = A<br>THD = 0.75% | Fundamental = 2481A<br>THD = 0.76% | Fundamental = 4837 A<br>THD = 0.18% |

Abbreviations: OWF-VSC, offshore wind farms voltage source converter (VSC); THD, total harmonic distortion.

By identifying the first subsystem, on the basis of Equation 5, with Equation 28, it can be yield:

$$\begin{aligned} \zeta_{13} &= V_{dc3}, \quad u_{13} = P_3, \quad y_{13} = h_{13} = V_{dc3} \\ L_{f_{13}}h_{13} &= \frac{i_{dc3}}{C_{eq3}}, \quad L_{g_{13}}h_{13} = \frac{-1}{C_{eq3}V_{dc3}}. \end{aligned} \tag{29}$$

The second and the third subsystems are built on the basis of the active and reactive power expressions. The derivative of Equation 27 yields

$$\begin{aligned} \frac{dP_k}{dt} &= -\omega_k Q_k + \frac{\omega_k \psi_{t\alpha k}}{L_s}\left(-R_s i_{\beta k} - \omega_k \psi_{t\alpha k} + v_{t\beta k}\right) \\ &\quad - \frac{\omega_k \psi_{t\beta k}}{L_s}\left(-R_s i_{\alpha k} + \omega_k \psi_{t\beta k} + v_{t\alpha k}\right) \\ \frac{dQ_k}{dt} &= \omega_k P_k + \frac{\omega_k \psi_{t\alpha k}}{L_s}\left(-R_s i_{\alpha k} + \omega_k \psi_{t\beta k} + v_{t\alpha k}\right) \\ &\quad + \frac{\omega_k \psi_{t\beta k}}{L_s}\left(-R_s i_{\beta k} - \omega_k \psi_{t\alpha k} + v_{t\beta k}\right). \end{aligned} \tag{30}$$

The identification of Equation 30 with Equation 28 leads to

$$\begin{aligned} \zeta_{2k} &= P_k, u_{2k} = \bar{v}_{t\alpha k} = \frac{\omega_k}{L_s}\left(-\psi_{s\beta k} v_{t\alpha k} + \psi_{s\alpha k} v_{t\beta k}\right) \\ y_{2k} &= h_{2k} = P_k, L_{g_{2k}}h_{2k} = 1 \\ L_{f_{2k}}h_{2k} &= -\omega_k Q_k + \frac{\omega_k \psi_{s\alpha k}}{L_s}\left(-R_s i_{\beta k} - \omega_k \psi_{s\alpha k}\right) \\ &\quad - \frac{\omega_k \psi_{t\beta k}}{L_s}\left(-R_s i_{\alpha k} + \omega_k \psi_{t\beta k}\right) \\ \zeta_{3k} &= Q_k, u_{3k} = \bar{v}_{t\alpha k} = \frac{\omega_k}{L_s}\left(\psi_{s\alpha k} v_{t\alpha k} + \psi_{s\beta k} v_{t\beta k}\right) \\ y_{3k} &= h_{3k} = Q_k, L_{g_{3k}}h_{3k} = 1 \\ L_{f_{3k}}h_{3k} &= \omega_k P_k + \frac{\omega_k \psi_{t\alpha k}}{L_s}\left(-R_s i_{\alpha k} + \omega_k \psi_{t\beta k}\right) \\ &\quad + \frac{\omega_k \psi_{t\beta k}}{L_s}\left(-R_s i_{\beta k} - \omega_k \psi_{t\alpha k}\right). \end{aligned} \tag{31}$$

In the following sections, the backstepping method will be used for developing the DC voltage and power controllers.

### 3.3.1 | DC voltage controller synthesis

The purpose of this control is to monitor the DC voltage to its reference, so the first tracking error is defined as

$$z_{13} = y_{13} - y_{13d}, \tag{32}$$

where $y_{13d} = V_{dc\_ref}$.

The differentiation of Equation 32 with respect to time yields to

$$\dot{z}_{13} = L_{f_{13}}h_{13} + L_{g_{13}}h_{13}P_{3_{ref}} - \dot{y}_{13d}. \tag{33}$$

Consider the Lyapunov function candidate given by

$$V_{13} = \frac{1}{2}z_{13}^2. \tag{34}$$

And its respective first time derivative is

$$\dot{V}_{13} = z_{13}\dot{z}_{13}^2 = z_{13}\left(L_{f_{13}}h_{13} + L_{g_{13}}h_{13}P_{3_{ref}} - \dot{y}_{13d}\right). \tag{35}$$

To ensure stability, the following command must be chosen:

$$P_{3_{ref}} = \frac{-k_{13}z_{13} - L_{f_{13}}h_{13} + \dot{y}_{13d}}{L_{g_{13}}h_{13}}, \tag{36}$$

where $k_{13}$ is appositive constant.

### 3.3.2 | Power controller synthesis

The control of active and reactive power is done on basis of the second and third subsystems. Their outputs must follow the paths that impose their references $P_{k\_ref}$ and $Q_{k\_ref}$.

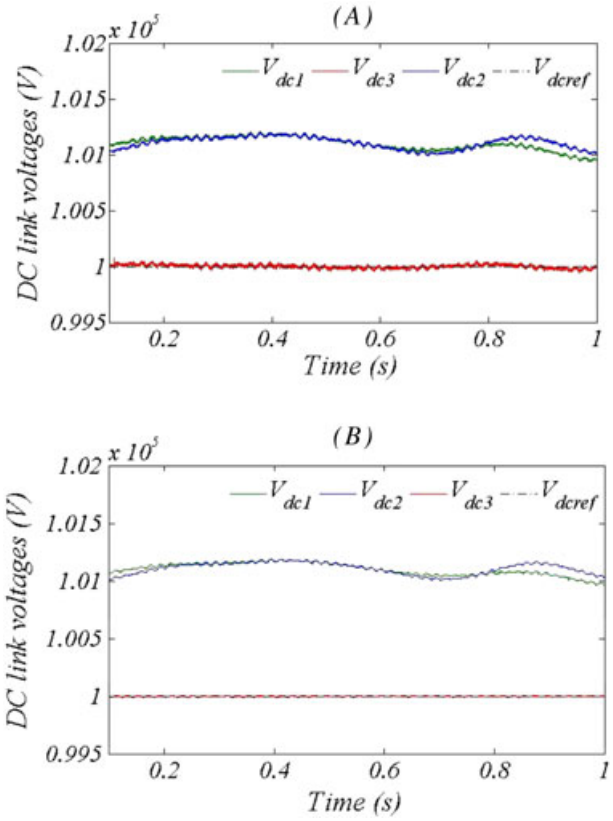


**FIGURE 7** Simulation results of DC-links voltages: (A) with PI control, (B) with backstepping control

The error variables are chosen as

$$\begin{aligned} z_{2k} &= y_{2k} - y_{2kd} \\ z_{3k} &= y_{3k} - y_{3kd}, \end{aligned} \tag{37}$$

where $y_{2kd} = P_{k\_ref}, y_{3kd} = Q_{k\_ref}$.

Their derivatives are given by

$$\begin{aligned} \dot{z}_{2k} &= L_{f_{2k}} h_{2k} + L_{g_{2k}} h_{2k} \overline{v}_{t\alpha k_{ref}} - \dot{y}_{2kd} \\ \dot{z}_{3k} &= L_{f_{3k}} h_{3k} + L_{g_{3k}} h_{3k} \overline{v}_{t\beta k_{ref}} - \dot{y}_{3kd}. \end{aligned} \tag{38}$$

Choosing the following Lyapunov functions

$$\begin{aligned} V_{2k} &= \frac{1}{2} z_{2k}^2 \\ V_{3k} &= \frac{1}{2} z_{3k}^2. \end{aligned} \tag{39}$$

By differentiating the Lyapunov functions with respect to time, it follows that

$$\begin{aligned} \dot{V}_{2k} &= z_{2k} \dot{z}_{2k} = z_{2k} \left( L_{f_{2k}} h_{2k} + L_{g_{2k}} h_{2k} \overline{v}_{t\alpha k_{ref}} - \dot{y}_{2kd} \right) \\ \dot{V}_{3k} &= z_{3k} \dot{z}_{3k} = z_{3k} \left( L_{f_{3k}} h_{3k} + L_{g_{3k}} h_{3k} \overline{v}_{t\beta k_{ref}} - \dot{y}_{3kd} \right). \end{aligned} \tag{40}$$

To make negative the derivatives of Lyapunov functions, the intermediate control laws $\overline{v}_{t\alpha k ref}$ and $\overline{v}_{t\beta k ref}$ are proposed in the following equation:

$$\begin{aligned} \overline{v}_{t\alpha k_{ref}} &= \frac{-k_{2k} z_{2k} - L_{f_{2k}} h_{2k} + \dot{y}_{2kd}}{L_{g_{2k}} h_{2k}} \\ \overline{v}_{t\beta k_{ref}} &= \frac{-k_{3k} z_{3k} - L_{f_{3k}} h_{3k} + \dot{y}_{3kd}}{L_{g_{3k}} h_{3k}}, \end{aligned} \tag{41}$$

where $k_{2k}$ and $k_{3k}$ are positive constants.

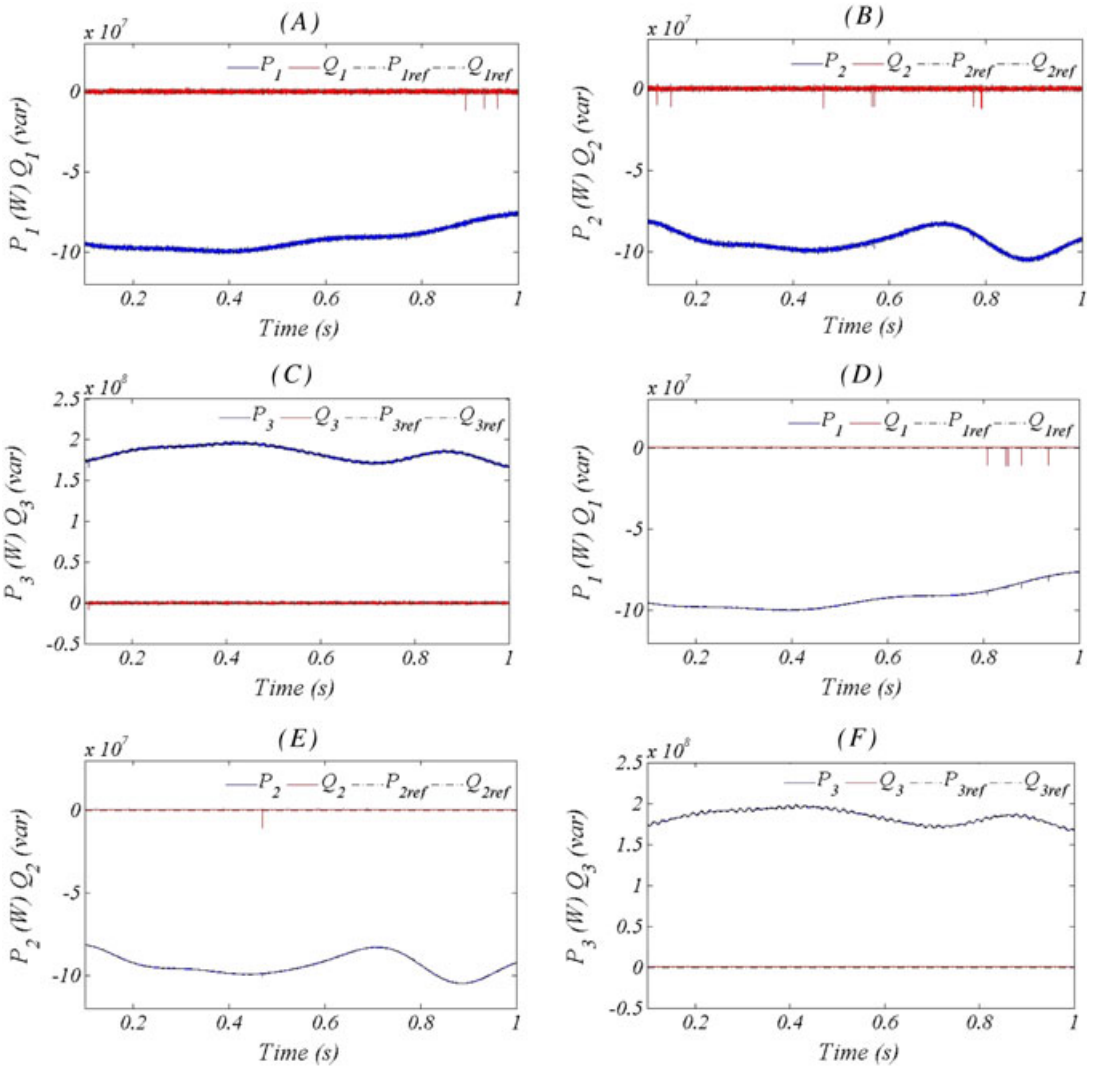


**FIGURE 8** Simulation results of active and reactive power: (A,B,C) with PI control, (D,E,F) with backstepping control

The final control laws are given by

$$\begin{bmatrix} v_{t\alpha k_{ref}} \\ v_{t\beta k_{ref}} \end{bmatrix} = \frac{\omega_k}{L_s} \begin{bmatrix} -\psi_{s\beta k} & \psi_{s\alpha k} \\ \psi_{s\alpha k} & \psi_{s\beta k} \end{bmatrix}^{-1} \begin{bmatrix} \overline{v}_{t\alpha k_{ref}} \\ \overline{v}_{t\beta k_{ref}} \end{bmatrix}. \quad (42)$$

## 4 | SIMULATION RESULTS

The 3 terminals VSC-HVDC system, shown in Figure 1, was simulated using Matlab/Simulink environment. There are two 100 MW OWFs connected to the VSC-MTDC network. The 3 VSCs use the 5-level T-type converter configuration. The rated DC voltage is 100 kV. DC cables were used to connect the 3 terminals, and each cable has the equivalent parameters of $R_{line} = 0.0699\ \Omega/km$, $L_{line} = 0.19\ mH/km$, and $C_{line} = 0.308\ \mu F/km$. The VSCs units operate at unity power factor. The rest of simulation parameters are gathered in Table 4.

### 4.1 | Step change of OWFs' power reference

Step changes of the input power were used to evaluate the control strategies. Table 5 illustrates the conditions of powers changes in the proposed test.

Figure 4 shows the results of DC-link voltage at each terminal. In the third terminal, the proposed control methods are able to maintain the voltage almost constant during the power changes. The DC-links voltages in the first and the second terminal are in proportion to the changes of the reference powers. It is evident from these results that the backstepping controller has given oscillations free transient response.

Figure 5 shows the dynamic response of the system under various step changes in active power demands of the MTDC system for PI and backstepping controllers, respectively. During this test, changes in active power references of OWF-VSC1 and OWF-VSC2 are introduced, whereas the reactive power references of all units are set to zero. It can be observed that the active and reactive power are very close to their references and are well decoupled from each other. Also, according to these results, it is worth to point out that the unity power factor operation is successfully achieved at different stations. Compared to the traditional PI control, a smaller overshoot and fast stabilization can be achieved under backstepping control.

As shown in Figure 6, the capacitor voltages on the DC bus are balanced before and after the power variations. It is important also to note that the application of the proposed redundant vectors-based 5-level SVM control maintains capacitor voltages balanced to their references.

Table 6 gives an idea about the harmonic spectrum of line currents. The total harmonic distortion values demonstrate that the distortions in line currents with backstepping controller are less than in the case of PI controller.

### 4.2 | Variation of OWFs'reference power

In this test, the reference power is chosen to imitate thereal wind variation.

Figures 7 and 8 present the responses of the multiterminal HVDC transmission system under variable reference power generated by the wind farms. From this response, it is clear that the control strategies give a good transmission of active and reactive power and regulate the DC voltage to its reference. On the other hand, the DPC combined with backstepping controllers behaves more efficient in reference power tracking compared to that with traditional PI controllers.

### 4.3 | OWF converter disconnection

In this case, the OWF-VSC1 is disconnected at 0.5 second, whereas the OWF-VSC2 remains injecting the same power level.

Before the disconnection, the system operates at nominal mode where the 2 OWFs delivered 100 MW. At time instant $t = 0.5$ second, OWF-VSC1 is disconnected, whereas the

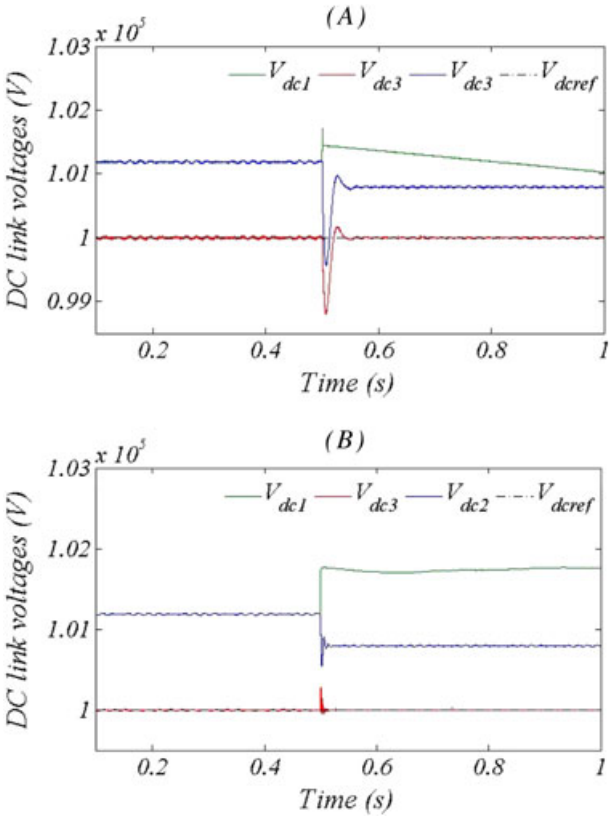


**FIGURE 9** Simulation results of DC-links voltages during converter disconnection: (A) with PI control and (B) with backstepping control

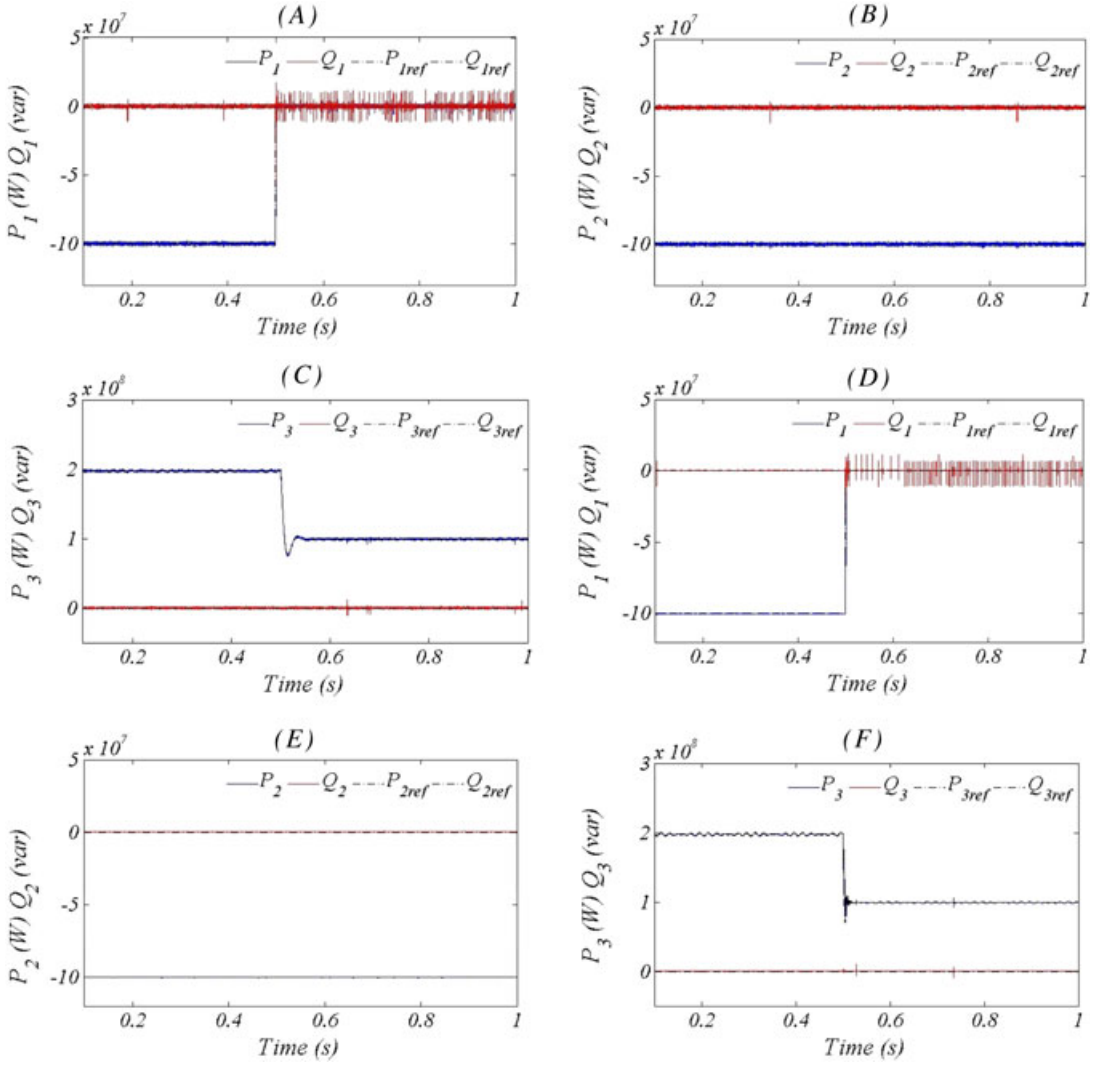


**FIGURE 10** Simulation results of active and reactive power during converter disconnection: (A,B,C) with PI control,(D,E,F) with backstepping control

OWF-VSC2 remains to inject the same power level. Figure 9 illustrates the DC voltage of each converter. It can be observed that the DC voltage is nearly constant and is regulated at its corresponding reference value.

As a consequence of the disconnection of OWF-VSC1, the proposed control method is active to regulate the DC voltage and ensure adequate transmission of the power generated in the OWF-VSC2, as shown in Figure 10.

It is clear from the disconnection test that the performance of the nonlinear controller is satisfactorily compared to its counterpart traditional PI controller.

## 5 | CONCLUSION

In this study, a VF-DPC based on backstepping approach has been proposed to control a 5-level T-type multiterminal VSC-HVDC transmission system. This study confirms that the proposed control scheme is able to control the power flow in a long distance as well as establish sinusoidal grid currents on sending and receiving ends with low harmonic distortion. Also, DC voltage regulation and capacitor voltages balancing are effectively achieved. Simulation results corroborate the capability of the proposed MTDC system to operate in disconnection mode. The comparison between the proposed nonlinear controller and the conventional PI controller points out the excellent performance of the backstepping control under various operating conditions.

## REFERENCES

1. Chen Y, Dai J, Damm G, Lamnabhi-Lagarrigue F. Nonlinear control design for a multi-terminal VSC-HVDC system. European Control Conference (ECC), Zürich, Switzerland, 3536-3541, July 17-19, 2013.
2. Liu B, Xu J, Torres-Olguin RE, Undeland T. Faults mitigation control design for grid integration of offshore wind farms and oil & gas installations using VSC HVDC. SPEEDAM 2010 International

Symposium on Power Electronics, Electrical Drives, Automation and Motion, 792-797, 2010.

3. Egea-Alvarez A, Beerten J, Van Hertem D, Bellmunt OG. Hierarchical power control of multiterminal HVDC grids. *Electr Power Syst Res*. 2015;121:207-215.
4. Sahu P, Acharya V. THD analysis of a VSC based HVDC transmission using multi-level converters and two-level converters. *Electron Instrum Eng*. 2013;2:6098-6105.
5. Meah K, Ula S. Comparative evaluation of HVDC and HVAC transmission systems. IEEE Power Engineering Society General Meeting, Tampa, FL, USA, 1-5, 24-28 Jun, 2007.
6. Gavriluta C, Candela I, Citroa C, Luna A, Rodriguez P. Design considerations for primary control in multi-terminal VSC-HVDC grids. *Electr Power Syst Res*. 2015;122:33-41.
7. Ramadan HS, Siguerdidjane H, Petit M, Kaczmarek R. Performance enhancement and robustness assessment of VSC-HVDC transmission systems controllers under uncertainties. *Electr Power Energy Syst*. 2012;35:34-46.
8. Bidadfar A, Nee HP, Zhang L, et al. Power system stability analysis using feedback control system modeling including HVDC transmission links. *IEEE Trans Ind Electron*. 2016;31:116-124.
9. Tang X, Lu DDC. Enhancement of voltage quality in a passive network supplied by a VSC-HVDC transmission under disturbances. *Electr Power Energy Syst*. 2014;54:45-54.
10. Wang GD, Wai RJ, Liao Y. Design of backstepping power control for grid-side converter of voltage source converter-based high-voltage dc wind power generation system. *IET Renew Power Gener.* 2013;7:118-133.
11. Chaves M, Margato E, Fernando Silva J, Pinto SF, Santana J. HVDC transmission systems: bipolar back-to-back diode clamped multilevel converter with fast optimum-predictive control and capacitor balancing strategy. *Electr Power Syst Res*. 2011;81:1436-1445.
12. Nayak N, Routray SK, Rout PK. State feedback robust controller for transient stability enhancement of VSC-HVDC transmission systems. *Procedia Technol*. 2012;4:652-660.
13. Wang L, Nguyen Thi MS. Comparative stability analysis of offshore wind and marine-current farms feeding into a power grid using HVDC links and HVAC line. *IEEE Trans on Power Delivery.* 2013;28:2162-2171.
14. Liang J, Jing T, Gomis-Bellmunt O, Ekanayake J, Jenkins N. Operation and control of multi-terminal HVDC transmission for offshore wind farms. *IEEE Trans Power Delivery.* 2011;26(4):2596-2604.
15. Fernão Pires V. João Fialho, and J. Fernando Silva "HVDC transmission system using multilevel power converters based on dual three-phase two-level inverters". *Int J Electr Power Energy Syst*. 2015;65:191-200.
16. Chaves M, Margato E, Fernando Silva J, Pinto SF, Santana J. HVDC transmission systems: bipolar back-to-back diode clamped multilevel converter with fast optimum-predictive control and capacitor balancing strategy. *Electr Power Syst Res*. 2011;81: 1436-1445.
17. Madhan Mohan D, Singh B, Panigrahi BK. Dynamic dead angle control of three-level voltage source converter based HVDC system. India International Conference on Power Electronics, New Delhi, 1-6, 28-30 Jan, 2010.
18. Martinez-Rodrigo F, de Pablo S, Carlos Herrero-de Lucas L. Current control of a modular multilevel converter for HVDC applications. *Renew Energy.* 2015;83:318-331.
19. Saeedifard M, Iravani R, Pou J. A space vector modulation strategy for a back-to-back five-level HVDC converter system. *IEEE Trans Ind Electron*. 2009;56(2):425-466.
20. Saeedifard M, Iravani R, Pou J. Analysis and control of DC-capacitor-voltage-drift phenomenon of a passive front-end five-level converter. *IEEE Trans Ind Electr.* 2007;54(6):3255-3266.
21. Bouzidi M, Bouafia S, Bouzidi A, Benaissa A, Barkat S. Application of backstepping to the virtual flux direct power control of five-level three-phase shunt active power filter. *Int J Power Electron Drive Syst*. 2014;4(2):173-191.
22. Colak I, Kabalci E, Bay R. Review of multilevel voltage source inverter topologies and control schemes. *Energy Convers Manage*. 2010;52(2):1114-1128.
23. Welchko BA, de Rossiter Correa MB, Lipo TA. A three-level MOSFET inverter for low-power drives. *IEEE Trans on Ind Electron*. 2004;51(3):669-674.
24. Gayathri Devi KS, Arun S, Sreeja C. Comparative study on different five-level inverter topologies. *Int J Electr Power Energy Syst*. 2014;63:363-372.
25. Blaabjerg F, Ma K. Future on power electronics for wind turbine systems. *IEEE JEmerg Sel Top Power Electron*. 2013;1(3):139-152.
26. Nguyen TD, Dzung PQ, Dat DN, Nhan NH. The carrier-based PWM method to reduce common-mode voltage for three-level T-type neutral point clamp inverter. IEEE 9th Conference on Industrial Electronics and Applications (ICIEA), Hangzhou, China, 1549-1554, 9-11 Jun 2014.
27. Lee JS, Lee KB. An open-switch fault detection method and tolerance controls based on SVM in a grid-connected T-type rectifier with unity power factor. *IEEE Trans Ind Electron*. 2014;61(12):7092-7104.
28. Schweizer M, Lizama I, Friedli T, Kolar JW. Comparison of the chip area usage of 2-level and 3-level voltage source converter topologies. In Proc. of the 36th Annu. Conf. of the IEEE Ind. Elec. Society (IECON 2010), Phoenix, USA, Nov. 2010.
29. Du C, Agneholm E, Olsson G. Comparison of different frequency controllers for a VSC-HVDC supplied system. *IEEE Trans Power Delivery.* 2008;23:2224-2232.
30. Cichowlas M, Malinowski M, Kazmierkowski MP, Sobczuk DL, Rodríguez P, Pou J. Active filtering function of three-phase PWM boost rectifier under different line voltage conditions. *IEEE Trans Ind Power Electron*. 2005;52(2):410-419.
31. Chaoui A, Krim F, Gaubert JP, Rambault L. DPC controlled three-phase active filter for power quality improvement. *Electr Power Energy Syst.* 2008;30:476-485.
32. Malinowski M, Jasinski M, Kazmierkowski MP. Simple direct power control of three-phase PWM rectifier using space vector modulation (DPC-SVM). *IEEE Trans Ind Electron*. 2004;51(2): 447-454.

33. Malinowski M, Kazmierkowski MP, Hansen S, Blaabjerg F, Marques GD. Virtual flux based direct power control of three phase PWM rectifiers. *IEEE Trans Ind Applicat*. 2001;37(4):173-191.
34. Hotait HA, Massoud AM, Finney SJ, Williams BW. Capacitor voltage balancing using redundant states of space vector modulation for five level diode clamped inverters. *IET Power Electr*. 2010;3(2):292-313.

**How to cite this article:** Reguig Berra A, Barkat S, Bouzidi M. Virtual flux direct power-backstepping control of 5-level T-type multiterminal VSC-HVDC system. *Int Trans Electr Energ Syst*. 2017;e2352. https://doi.org/10.1002/etep.2352